Bachelor Project: The effect of an inhomogeneous medium on the ram pressure stripping of dwarf galaxies

Marten Blaauw

May 7, 2009

1 Introduction

There are mysterious interactions happening in our neighbourhood between orbiting dwarf galaxies and their surroundings. Theories about the influence of the environments of progenitor halos on their orbiting satellites have been developed and ram pressure stripping is one of them. Ram pressure stripping is a process of removing the cold gas component from the disks of satellites due to a hotter and less dense background media. The ram pressure forces come from the hot medium surrounding the progenitor galaxy according to a model developed from the early work of Gunn & Gott [11]. A clear example of such formalism applied to an orbiting galaxy within a cluster halo can be found in Abadi et al.[1]. Dressler [6] did a study of the galaxy populations in 55 rich clusters and examined the morphology and the distance from the cluster core. He found a well-defined relationship between the galaxies morphological type and the density of its surroundings, the so-called morphology-distance relation. In the dense environments near the clusters core, galaxy morphologies are mostly dominated by elliptical and S0, while on the less dense outskirts regions of the clusters the presence of spiral galaxies is larger. The difference in populations of spirals and ellipticals can be explained in terms of evolution: meaning that gas-rich spirals in the outskirts turn into S0's when falling into denser environments and lose their gas due to physical processes (Gunn & Gott [11]).

On smaller scales, the same evolutionary process seems to take place. The orbiting dwarf galaxies bound to the Milky Way (MW) can roughly be divided in two groups. According to a recent paper by Grcevich and Putman [9] who examined the HI content and environment of many dwarf galaxies including many newly discovered satellites in the MW and M31, most dwarf galaxies within $\sim 270\ h^{-1}$kpc are gas-poor pressure supported dwarf galaxies, dSphs. The dSphs are the least luminous dwarfs ($M_b \sim -9$), show very little or no rotation and consist of old stellar populations (Grebel, Gallagher and Harbeck [10]). Outside $\sim 270\ h^{-1}$kpc, most dwarf galaxies have a detectable HI content, consist of young stars and are rotational supported by their disk, dIrr's. Besides the environments where they are found, there are other signs for evolution in morphology from dIrrs to dSphs:

1. dSphs and dIrrs have similar exponential radial brightness profiles (Lin & Faber [17]) meaning that they could be the same basic type of galaxy.

2. Some dSphs show extended star formation histories (Hernandez et al. [12]) which mean that their progenitors were gas-rich.

3. a few galaxies are found with properties of both dIrrs and dSphs (Grebel, Gallagher and Harbeck [10])

In order to evolve from dIrr galaxies to dSph galaxies: (1) gas has to be stripped off the disk of the dIrr to the environment and (2) rotation has to be suppressed turning a rotation supported system into a pressure supported system. There have been proposed several mechanisms able to transform dIrr onto dSphs. For instance, based on gravitational effects, like tidal stripping and tidal stirring (Mayer et al. [21], [22] & [23]), where tidal stripping describes the removal of cold gas from the disk by tidal shocks (1) and tidal stirring reduces the angular momentum of dIrrs (2).

Environmental effects, such as ram pressure or galaxy starvation, might also play an important role on the morphology transformation on satellite galaxies. The nature of the environment surrounding the MW is still unclear, although there are observational hints of a hot halo component equivalent to the one detected in galaxy cluster environments. First, X-ray absorption lines are detected that are likely produced by local hot gas near $\sim 50\ h^{-1}$kpc (Fang et al. [8]). Further, indirect arguments come from the success of ram pressure stripping models on, for example, the Magellanic stream (Mastropietro et al. [20]). Besides ram pressure stripping, the environment can also remove gas by the process of galaxy starvation which removes the diffuse hot outlying gas from spirals (Larson et al. [15]) rather than the cold gas from the disk component.

It's likely that the evolution occurs due to both gravitational tides and hydrodynamic processes due to the environment. Mayer et al. [23] show that ram pressure forces alone are not efficient enough for dwarf dark halo's with $V_{peak} \geq 30$ km s^{-1}. The combination of tides and ram pressure stripping is in general more effective than each alone as tidal forces lowers the value of V_{peak} and as a result ram pressure forces strip more cold gas from the dwarfs disk.

In this report we will focus on the outskirts of the MW and on the dark halo dominated progenitors of today's dSphs. For those dwarfs with pericenter passages at this long distance, the effects of tidal forces are small compared to ram pressure forces. Furthermore, tidal stirring is ineffective for less luminous dIrrs dominated by their own dark halo's (Mayer et al. [23]). Therefore, we focus our analysis on the ram pressure stripping as being the main mechanism responsible for morphological changes on dwarf galaxies orbiting the external regions of their host halos.

The assumption of a homogeneous distribution of the hot background medium is commonly used. As a result, the effectiveness of ram pressure forces depends only on the distance to the centre of the host and masses of the dwarfs. For the most far away isolated dSphs like Leo I, Tucana, Cetus and Pegasus this means they have to be on very eccentric orbits in order to be stripped off their gas effectively. The constraints on initial orbits and masses can be lowered by considering an inhomogeneous background medium, like the complex multiphase structure model (Maller & Bullock [19]). The progenitors of dSphs could have move through clumpy media and experienced a larger ram pressure stripping than predictions from homogeneous background models at those distances. On cluster scale, there is observational evidence of the inhomogeneity of the background gas (Tonnesen & Bryan [30]). In this paper we will assume an inhomogeneous medium and investigate its effect on the ram pressure stripping of dwarf galaxies.

The outline is as follows. In chapter 2, the initial dwarf galaxy models and the model of the host galaxy are given and are used to examine the conditions for effective ram pressure stripping in the case of a homogeneous medium. Numerical techniques are given in chapter 3 to examine the inhomogeneity of the medium. At the end of chapter 3 we combine these results with the initial models from chapter 2. Our final results are summarized and discussed in the discussion and conclusion section.

2 Homogeneous background model

Using an analytical approach, the conditions are explored in this section under which satellites orbiting a host halo are effectively depleted of their cold gas content by ram pressure forces. Our approach uses assumptions of symmetry and homogeneity on the background hot gas distribution. Those hypotheses commonly imply that the gaseous component of the host halo is distributed smoothly following a given density profile that depends only on radius. Whether this gas will strip the cold gas content from satellites by ram pressure forces or not depends on a few parameters:

1. The gravitational resistance of the infalling dwarf galaxy.
2. The inclination of the infalling dwarf galaxy
3. The motion and the density of the background medium surrounding the dwarf galaxy.

Such conditions will be considered and discussed for this analytical model.

2.1 The host galaxy

The host galaxy is assumed to have comparable properties than the Milky Way (MW). In this homogeneous background model the density of the dark matter (DM) halo is a function of radius only. The density profile of DM will be described with a NFW profile (Lokas [18]; Navarro, Frenk & White [26]):

$$\rho(s) = \rho_c^0 \frac{vc^2 g(c)}{3s(1+cs)^2} \tag{1}$$

where

$$g(c) = \frac{1}{ln(1+c) - \frac{c}{1+c}} \tag{2}$$

is a function of the concentration parameter c only and where

$$s = \frac{r}{r_{vir}} \tag{3}$$

where r_{vir} is the virial radius of the halo. The virial radius is defined here as the distance from the halo centre where the mean density of a sphere with radius

r_{vir} is v times the critical density ρ_c^0. v is the virial overdensity (Bryan & Norman [3]). ρ_c^0 is the current critical density. The used values of these parameters for this model are given in Table 1. The resulting value for the virial radius is $r_{vir} = 205\ h^{-1}$kpc.

parameter	value
M_{vir}	1.0e12 $M_\odot$
c	10.0 h^{-1}kpc
v	100
ρ_c^0	277.5 $M_\odot$ kpc^{-3}

Table 1: The virial mass M_{vir} is given a value similar to the virial mass of the MW. The concentration parameter c is chosen to be the lower limit from the concentration-virial mass relation (Bullock et al. [4]). This results in an upper limit on the density in the outer regions. The value of the virial overdensity v is representative for a ΛCDM universe. Finally, the current critical density ρ_c^0 is calculated for the same type of universe.

In this model, the hot gas in the halo is assumed to follow an NFW profile within the virial radius. This NFW profile is calibrated using a density value of 10^{-4} cm^{-3} at 50 h^{-1}kpc as suggested by several observational constraints (see Mastropietro et al. [20] and references therein). For this profile the total mass of the hot gas within the virial radius equals $2 \times 10^{10}\ M_\odot$.

The hot gaseous halo exerts a pressure on the infalling dwarf galaxy thus its density profile is very important. However, little is known about the structure of hot gas in galactic halos. On larger scales, the structure of hot gas in groups and cluster-size systems is known from X-ray observations. The virial temperatures are larger ($T_{vir} > 10^7$ K) and emission from the hot halos is detectable in X-ray experiments. Supported by observational evidence, so-called β-profiles describe (Cavaliere [5]; Eke et al. [7]) the distribution of intracluster gas by $n_g(r) = N_{g,0}[1 + (r/r_c)^2]^{-3\beta/2}$ including a central core of constant density r_c. These distributions are obtained when some source of pre-heating is present and are usually referred as 'high-entropy' profiles, in contrast with a cuspy distribution or 'low-entropy' case.

Unfortunately, X-ray data is not available yet for the cooler environments in the MW halo. The projected densities of the halo and the correlated luminosities have too low values to be detectable. In a paper of Kaufmann [14], a pair of SPH simulations are used to examine the low- and high-entropy hot gaseous halo. In the low entropy case: cold gas collapses in the early universe without any pre-heating source and it follows the dark matter. The low-entropy halo cools rapidly in time and its core becomes more than 10 times denser than the high-entropy halo core. In the high entropy case: gas is pre-heated during the collapse in the early universe by external resources. The high-entropy halo has a cored density profile. The gas in the high-entropy profile has a more extended structure and seems to have more dense clumps even beyond the virial radius. The differences between both profiles are large in the halo centre but roughly of the same order of magnitude near the virial radius. There is no compiling evidence supporting either of these two scenarios for galactic-sized halos. Therefore, we will assume the simplest profile where the gas follows the dark matter profile i.e. the low entropy case. As the NFW profile falls off more quickly in the outer regions compared to the high-entropy case (Fig. 6 in Kaufmann et al. [14]), the value assigned to the background gas density can be underestimated by a factor ≤ 3 (see Fig. 6 in Kaufmann et al.)

Besides the shape of the density profile, the calibration point at $r_{per} = 50$ h^{-1}kpc is also controversial. Mastropietro et al. [20] use a similar model in their paper in order to study the formation of the Large Magellanic Cloud (LMC) stream. They use a mass of 10^{10} $M_\odot$ for the hot gaseous halo and calibrate the profile assuming a particle density of 8.5×10^{-5} cm^{-3} at 50 h^{-1}kpc. In general, particle densities are constraint by others authors in the range of $10^{-4} - 10^{-5}$ cm^{-3} for distances in the range of $50 - 100$ h^{-1}kpc (Sembach et al. [28]; Putman et al. [27]). Grcevich et al. [9] estimated higher densities constraints between $2 - 3 \times 10^{-4}$ cm^{-3} out to distances of at least 70 h^{-1}kpc. These authors examined the HI content and environment of all of the Local Group dwarf galaxies. They combined ram pressure arguments with velocities from proper motion studies to estimate the halo density of the MW at several distances. Lower values for the halo density are from Murali [25] where an upper limit of $n_h < 10^{-5}$ cm^{-3} is estimated. We assume in our model a value of 10^{-4} cm^{-3} at $r = 50$ h^{-1}kpc, which is within the (wide) range of observational values reported so far by other authors.

2.2 The satellite galaxy

The satellite galaxy is modelled with 2 components: the dark matter halo and the disc. The contribution of the bulge is negligible and will not be included. The gravitational resistance of the bulge is only relevant near the core of the dwarf while we focus more on gas removal from the disc. The disc is assumed to be axisymmetric and has an exponential density distribution:

$$\rho_d(R, z) = \frac{M_d}{4\pi R_d^2 z_d} \exp(\frac{-R}{R_d}) \mathrm{sech}^2(\frac{z}{z_d}) \tag{4}$$

Where R_d is the radial scale length, z_d is the vertical scale length and M_d is the disc mass of both gas and stars.
The density profile of the satellite galaxy halo is given by a Hernquist [13] profile:

$$\rho_h(r) = \frac{M_h a}{2\pi r (r + a)^3} \tag{5}$$

Where a is the scale length and M_h is the total mass of the dwarfs halo.

We use predictions from semi-analytical models within the ΛCDM scenario in order to fix the mass parameters in these formulas. We selected a sample of ~ 300 undisturbed dIrr galaxies falling into one MW-like from the GA2 simulation (Stoehr et al. [29]; Li et al. [16]). The average mass of the DM halos for these objects is $M_v \approx 10^9$ $M_\odot$ corresponding to faint dIrr galaxies and is similar to the mass of the DM halo used in the GR8 model (Mayer et al. [21]). The left histogram shows the distribution of the virial masses of dIrr galaxies. With the distribution of DM known, semi-analytic input has been used in the

GA2 simulation to model the baryonic properties through equations instead of simulating the complex physical processes between baryons. The middle and right histograms show the resulting distributions of the gas and stellar masses. The median values for the virial mass M_v, the cold gas mass M_{cg} and the stellar mass M_{st} are shown in Fig. 1 as vertical lines.

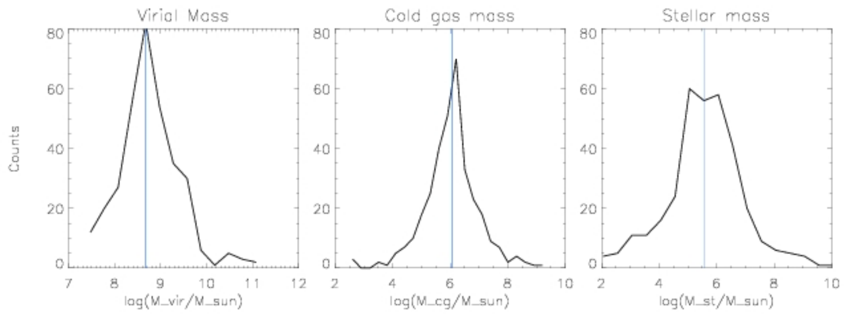

Figure 1: Histograms of the virial mass M_v in $M_\odot$, the cold gas mass M_{cg} in $M_\odot$ and the stellar mass M_{st} in $M_\odot$. The data comes from an example of ≈ 300 undisturbed infalling dwarf galaxies from a GA2 + semi-analytic simulation (Stoehr et al. [29]; Li et al. [16]). The vertical lines divide the three graphs in two equal sized areas. Their mass values are used for the dwarf galaxy model parameters.

The resulting values from Fig. 1 will be used in our analytical model for ram pressure and are given in table 2 using $M_d = M_{st} + M_{cg}$ and $M_h = M_v - M_d$. The scaling parameters are also given in table 2.

2.3 Ram pressure

The equations of the models from previous sections will be used for the analytic description of ram pressure stripping. According to the early ideas of Gunn & Gott [11] cold gas is being removed from the disc when ram pressure due to the background is greater than the gravitational restoring force per unit area provided by the disc and halo of the dwarf galaxy (halo component also included in Mayer [23]). Ram pressure from the background is given by:

component	parameter	value
Halo	Mass dark matter (M_h)	4.7e8 $M_\odot$
	Scale length (a)	5.0 h^{-1}kpc
Disc	Mass stellar and gaseous disc (M_d)	1.5e6 $M_\odot$
	Cylindrical scale length (R_d)	1.0 h^{-1}kpc

Table 2: The value of the cylindrical scale length R_d is based on the one from the LMC (Mastropietro [20]). We use for the halo a Hernquist profile with scale length $a = 5\ h^{-1}$kpc.

$$P_{ram} = \rho v^2 \tag{6}$$

where ρ is the density of the background and v is the velocity of the dwarf galaxy with respect to the background.
This force will be (partially) cancelled out by the gravitational resistance provided by the dwarf components. This gravitational restoring force per unit area is calculated analytically and is simplified by aligning its z coordinate in the opposite direction of v. By assuming this face-on motion the gravitational resistance can be calculated directly from:

$$P_{grav,i} = \frac{\partial \phi_{grav,i}}{\partial z}(R,z)\sigma_{grav,i}(R) \tag{7}$$

For each dwarf component i where $\frac{\partial \phi_{grav,i}}{\partial z}(R,z)$ is in the opposite direction of v. Mayer [23] numerically estimated the effect of inclination on ram pressure. Minimal stripping occurs for an edge-on passage and maximum stripping occurs for a face-on passage. During its journey through the hot gaseous halo the inclination with respect to the background changes continuously. Thus our face-on assumption results in an upper limit for the ram pressure experienced by the dwarf.

Both the halo and disc potential of the dwarf galaxy contribute to P_{grav}. The total gravitational potential ϕ_i of a galaxy component i can be derived from the Poisson equation $\nabla^2\phi(R,z) = 4\pi G\rho(R,z)$. The derivation of ϕ_i with respect to z yields the acceleration of a particle due to the restoring gravity from component i. The acceleration in the z-direction is at maximum for the face-on case. For the halo this term is equal to (Hernquist):

$$\frac{\partial \phi_h}{\partial z}(R,z) = \frac{GM_h}{(\sqrt{R^2+z^2}+a)^2}\frac{z}{\sqrt{R^2+z^2}} \approx \frac{GM_h z}{(R+a)^2 R} \qquad z \ll 1 \tag{8}$$

And for the disc (Binney & Tremaine [2]):

$$\frac{\partial \phi_d}{\partial z}(R,z) = GM_d \int_0^\infty \frac{J_0(kR)\exp(-k \mid z \mid)}{[1+(kR_d)^2]^{\frac{3}{2}}} k dk \tag{9}$$

Where the first order Bessel function $J_0(kR) = \pi^{-1}\int_0^\pi \cos x \sin\Theta d\Theta$.

The second term of equation (7) is the surface density and can be derived from the density profile of component i:

$$\sigma_i(R) = \int_\infty^\infty \rho_i(R,z)dz \tag{10}$$

For the halo we get this by combining the equations (5) and (10). The disc is not as simple, and an approximation has been used here (Binney & Tremaine [2]):

$$\sigma_d(R) = \frac{M_d}{2\pi R_d^2} \exp(\frac{-R}{R_d}) \tag{11}$$

The satellite stripping is therefore determined by the interplay between its gravitational resistance (Eq. (7)) and the pressure provided by the background conditions (Eq. (6)) and it can be studied by solving the following equality:

$$\rho v^2 = \sum_i \frac{\partial \phi_{grav,i}}{\partial z}(R,z)\sigma_{grav,i}(R) \tag{12}$$

For any given radius R and background parameters v and ρ, the gravitational resistance of the dwarfs components is inversely proportional to the height above the disks plane, z, and is maximum in the plane of the disc. We will therefore restrict our analysis to such case, or equivalently, to the "infinitesimally thin" disk approximation, which allows us to compute the gravitational resistance as only a function of R. We made two further approximations: (i) as stated before, we consider only face-on motions and (ii) we compute "instantaneous" ram pressure forces, which means we do not study its variation along the orbit of the satellite within the host potential. Instead, our calculations must be interpreted as the ram pressure forces experienced at the pericenter passages, where the background density is at maximum. Given these 3 restrictions, we can calculate the stripping radius, R_{sp}, at which the ram pressure effectively removes all gas content with $R > R_{sp}$ from the disk of the dwarf galaxy.

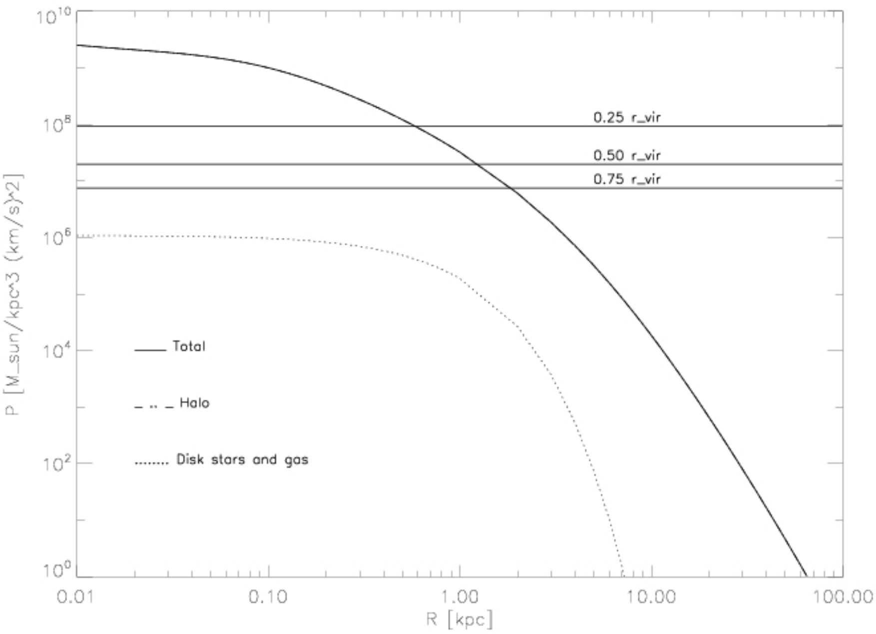

Figure 2: Gravitational resistance force per unit area for the halo (dash-dot) and disc (dot) component and the sum of both components (line), as a function of cylindrical radius R. The disc is assumed to be axisymmetric and exponential. A Hernquist profile has been used for the halo (Table 2). The three horizontal lines represent ram pressure values at fixed velocity of 200 km s^{-1} at pericenter passages: $[0.25, 0.50, 0.75]$ r_{vir}. The values for the background densities are respectively: $[1.0 \times 10^{-4}, 2.0 \times 10^{-5}, 7.6 \times 10^{-6}]$ cm^{-3}.

In Fig. 2 the curved lines show the total gravitational restoring force per area together with the contribution of each of the satellite components as a function of the (cylindrical) radius R within the dwarf. The horizontal lines represent the ram pressure values at three different pericenter radii using our model described in section 2.1. The intersection between the curved and the horizontal lines show the location of the stripping radius, R_{sp}. At a radius $R > R_{sp}$ cold gas is being removed from the disk and at $R < R_{sp}$ it remains bound to the dwarfs disk. Fig. 2 shows that at fixed velocity, the removal radius is smaller the closer the pericenter passage. Notice that the dark matter is the main contributor to the gravitational potential. The amount of DM mass is more than two orders of magnitude larger than the baryonic mass. The dark matter contribution is what makes the dwarfs disks being more resistant to gas depletion. This implies that the dark matter contribution plays a fundamental role in damping the effects of tidal stripping (Mayer et al. [21]) and also reduces the effects of ram pressure stripping. Therefore, dwarfs are able to maintain a larger fraction of fresh fuel for star formation instead of losing and incorporating it to the host reservoir.

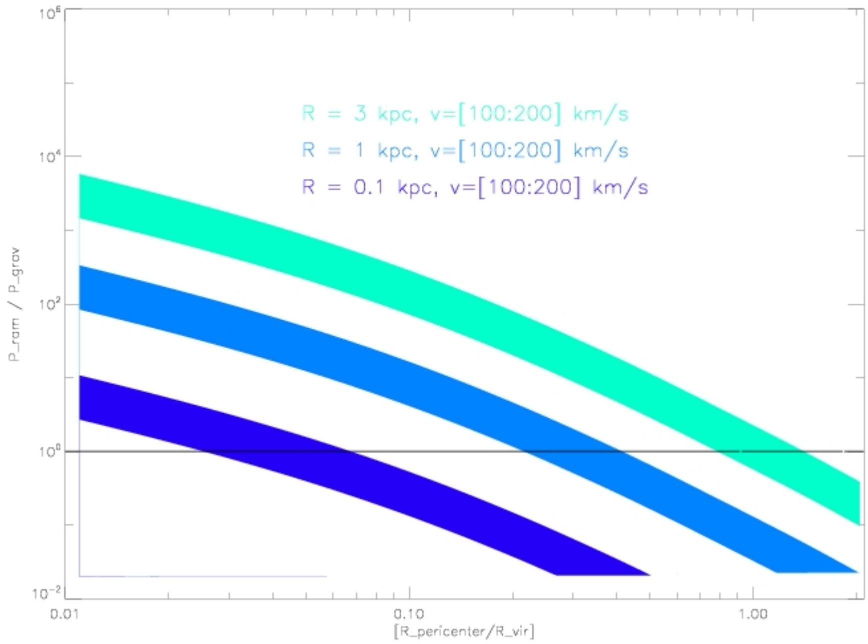

Figure 3: Ratio of ram pressure and gravitational restoring force as a function of the pericenter radius as a fraction of the virial radius, $r_{vir} \approx 200\ h^{-1}$kpc. The division of the pericenter radius by the virial radius is done to make an easier comparison with the numerical results. The gravitational restoring force is calculated for three different radii, $R = [0.1, 1.0, 3.0]\ h^{-1}$kpc. The ram pressure is calculated as a function of pericenter radius using a NFW profile for the hot gaseous halo. A particle density value of ($\rho_{obs} = 10^{-4}$ cm^{-3}) at 50 h^{-1}kpc or 0.25 r_{vir} is used as a calibration point. Finally, the three areas reflect the given range of velocities for each R.

In Figure 3 the ratio of the competing ram pressure and gravitational resistance is plotted as a function of the pericenter radius (normalized to $r_{vir} \sim 200$ h^{-1}kpc). For $R = 1\ h^{-1}$kpc and $v = 100$ km s^{-1} the value of this ratio approximately equals one. The ram pressure and gravitational forces are comparable to each other here in agreement with Fig. 2. At this radius within the dwarf, the maximal pericenter radius for ram pressure to be effective is 0.25 r_{vir}, for larger pericenters the gravitational resitoring forces will prevent any gas removal at $R = 1\ h^{-1}$kpc. As the pericenter passages approach the virial radius, ram pressure forces become less effective, and only cold gas sitting in the outskirts of the dwarf disc ($R > 3R_d \sim 3\ h^{-1}$kpc) can be affected.

After investigating the three parameters mentioned in the introduction of this chapter our analytical model shows that:

1. Given the parameters for the dwarf galaxy model, it is clear that the dwarf halo is mainly responsible for the gravitational potential. The contribution of the disk mass is very small. The halo mass has a high influence on the stripping radius. When the amount of halo mass is *one* order of magnitude

larger, the needed ram pressure to remove all gas from the dwarf in the most innerparts ($R = 0.01\ h^{-1}$kpc) has to increase with *two* order of magnitudes.

2. For our model we assume a face-on approach of the dwarf galaxy through the progenitor halo yielding an upper limit to the ram pressure. For a more detailed discussion about the effects of inclination the reader is referred to Mayer et al. [23].

3. The properties of the background density and velocity are difficult to estimate. In our model the hot gaseous halo is assumed to follow a NFW profile where the particle density at 0.25 r_{vir} equals $\rho_{50} = 10^{-4}$ cm^{-3}. This value is chosen to be in the range of observational constraints for the MW halo. For such model, stripping of cold gas in the dwarf galaxies occurs mostly in small pericenter passages due to the increase of the background density of the host. Fig. 2 show that dwarf galaxies with velocities $100 - 200$ km s^{-1} do not lose their cold gas content within R_d for pericenter passages larger than $0.2 - 0.4\ r_{vir}$. Thus according to our model, dSph galaxies observed at or beyond r_{vir} like Leo I would have had a small pericenter passage in the past to lose its cold gas content. Another explanation for the absence of cold gas in dwarf galaxies comparable to Leo might be inhomogeneities in the hot gaseous halo. We investigate this possibility in the next chapter.

3 Inhomogeneous background model

Using results from numerical simulation provides more insight into the detailed structure of the hot gaseous halo. We combine information about the inhomogeneities expected on the background hot media of a simulated host halo with the analytic results from previous chapter in order to estimate the importance of inhomogeneity in the ram pressure stripping of infalling dwarf galaxies.

3.1 SPH simulation

We use an Nbody/SPH numerical simulation in order to characterize the clumpyness expected in the hot halo. We had selected a MW-size halo from a cosmological simulated box at $z = 2$[1]. We work under the assumption that the density contrasts found in such halo can be extrapolated to a halo of the same size at z=0, after proper re-scaling of the background density conditions. The halo has a total number of 172.175 dark matter particles and 84.352 baryonic particles within the virial radius, and the spatial resolution of the simulation is 0.5 h^{-1}kpc. Table 3 summarizes the relevant properties of the selected halo.

[1]This simulation is part of the Overwheningly Large Simulation (OWLS) project (Schaye et al. in preparation)

parameter MW type galaxy	value
R_{vir}	90 kpc
M_{vir}	1.2e12 M_{sun}
T_{vir}	2.1e6 K

Table 3: Basic parameters from the simulated halo. T_{vir} is defined as $37V_{vir}^2$, where V_{vir} is the radial velocity at virial radius.

All the resulting distances and masses are given in physical coordinates and made dimensionless by taking the ratio to the virial parameters. This makes it easier to compare the simulation results with the analytical ones introduced in Sec. 2. The next step is to define a criterion to divide between the hot and cold gas phases. Based on a visual inspection of the temperature distribution, we assume the criterion to be $T_{crit} = 0.06 * T_{vir} = 1.2 \times 10^5$ K. This threshold value will be used throughout the report to distinct between cold and hot gas particles. Fig. 4 shows the distribution of both components.

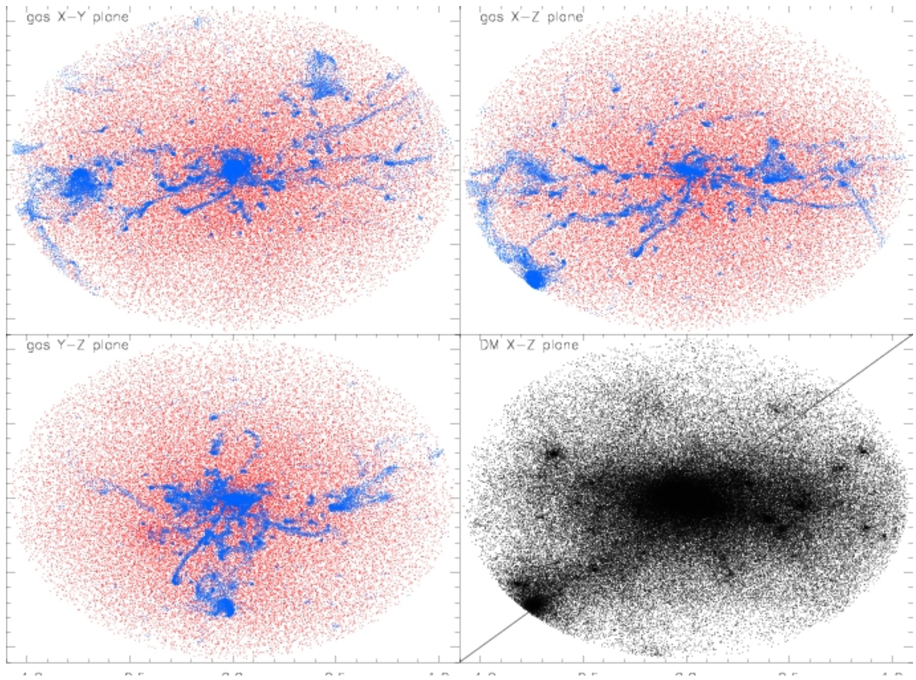

Figure 4: The two upper and the lower left subplots show the distribution of hot and cold gas particles in three projections at $z = 2$. The red dots represent 43.922 hot particles ($> T_{crit}$) which are distributed smoothly. The blue dots represent 40.430 cold particles ($< T_{crit}$) which show a clumpy distribution and are mainly concentrated in the centre. The criterion temperature is $T_{crit} = 0.06T_{vir}$. In the outer regions some streams of cold gas are visible indicating locally high density regions. The lower right figure shows the distribution of dark matter particles projected in the X-Z plane.

The density profiles of hot, cold and dark matter particles is calculated as the average density per shell. Fig. 5 shows the resulting profiles. The average density per shell depends on the radius and doesn't give information about the exact location of the inhomogeneities. However, it is useful to compare this result with the analytical assumptions made in the Section. First, it shows that hot particles are smoothly distributed while the cold ones tend to cluster together at the galactic centre. Second, the hot particles don't seem to follow the dark matter profile as its slope is less steep. Instead, the hot gas seems to follow a high-entropy profile as Fig. 5 shows an extended hot component. According to Kaufmann et al. [14] an initial high-entropy condition might result in a large number of fragmented cool clouds. These clouds are fragmented and pressure supported and are visible as the overdense cold gas regions in Fig. 4. The typical temperature of 10^4 K for the cool clouds and 10^6 K for the smooth component are in agreement with the results of Kaufmann for the high-entropy case.

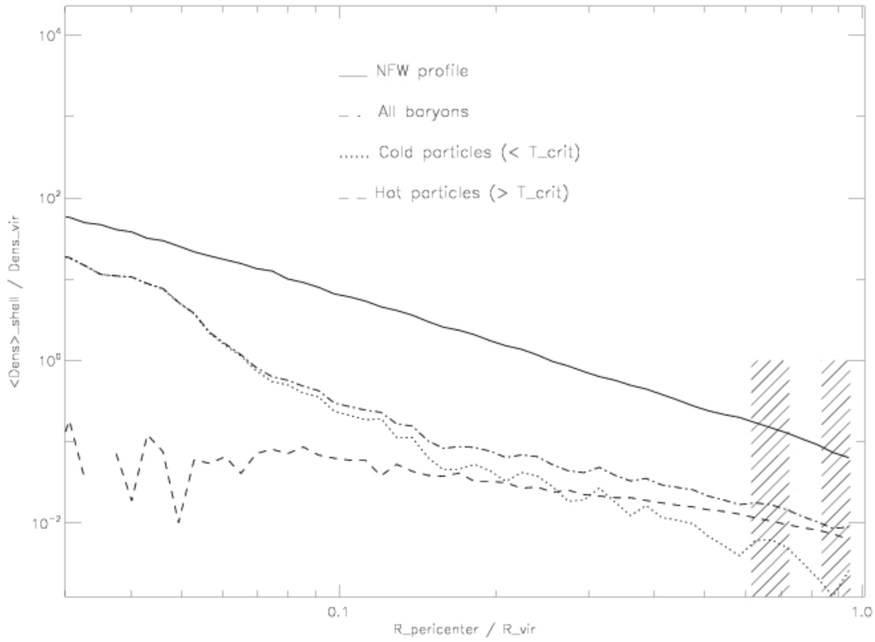

Figure 5: Density profiles for hot, cold, all baryonic and dark matter particles, where $T_{crit} = 0.06 * T_{vir}$ is the criterion between hot and cold particles. 80 Shells were used with logarithmic widths. The two vertical shaded area indicates the shells at $0.67R_{vir}$ and $0.89R_{vir}$ which are used in Fig. 6 to examine the local overdensities in the outer regions.

3.2 Local inhomogeneity

The two shells illustrated in Fig. 5 are chosen to examine the inhomogeneity of the background. The reason for choosing these shells in the outer regions is that we want to explore inhomogeneities at larger radii, where the ram pressure forces from a homogeneous medium is inefficient (see Sec. 2). We choose the following shells:

1. Shell 1: $0.61 < \frac{R}{R_{vir}} < 0.73$, # particles: 8.765
2. Shell 2: $0.80 < \frac{R}{R_{vir}} < 0.98$, # particles: 7.620

Given the number of particles (N) in each shell, the local density of each particle is calculated as follows:

Around each particle i, a sphere of radius R_i is drawn. R_i must not be chosen too small. It has to be representative for the size of the fragmented cool clouds. Too small values could result in very high densities locally but the size of the sphere would be too small to strip gas from the dwarf effectively. Also it would result in zero or a few particles within the sphere due to the mass resolution. On the other hand, too large values of R_i could result in too low density values due to averaging as the high densities of the fragmented clouds would be averaged out by its surroundings. We choose a value of $R_i = 3\ h^{-1}$kpc here which is equal to 3 times the typical disc scale length of dwarf galaxies and encloses 80% of the discs mass using our analytic model. The density of the sphere, ρ_i, is calculated by summing up all masses within this sphere and dividing by the spheres volume. The values of ρ_i are divided by the average density of the extended shell, ρ_{shell}. This extended shell includes: *both* the shell where all particles i are selected from (width: 10 h^{-1}kpc) *and* the surrounding shell of width $R_i = 3\ h^{-1}$kpc where particles are used for the calculation of ρ_i for each i near the edge of the main shell. The ratio Δ_i for all i in a given shell is calculated from:

$$\Delta_i = \frac{\rho_i}{\rho_{shell}} \tag{13}$$

This formula is applied to all particles in the two given shells.

Particles i in overdense regions (large Δ_i value) are of interest here. However, those overdense regions could be either an indication for the presence of a satellite galaxy, or overdensities on the background distribution. Satellite galaxies are not of interest as we do not take galaxy encounters into account here. Thus these halo dwarfs have to be identified and removed. Therefore, we remove particles with SFR $\neq 0$ and all particles within a spherical region of radius, R_{rem}, around them. We choose a removal radius of $R_{rem} = 3\ h^{-1}$kpc which is equal to 3 times the typical disc scale length of dwarf galaxies from our analytical approach. For the remaining particles eq. 13 is used again for calculating the ratio values where ρ_{shell} also takes the removed particles into account. In order to estimate the effects of this 'satellite galaxy' removal, we compare measurements of Δ in a set of particles that includes and excludes the removal of the identified dwarfs (Figure 6). The discrepancy starts to grow after $\Delta = 20$, indicating that highest Δ values are likely associated to satellite galaxies and are not representative of density fluctuations on the background media.

We will therefore exclude those values from our calculations. The remaining Δ values are associated to the halo gas background and are assumed to be capable of effective cold gas stripping on infalling dwarfs.

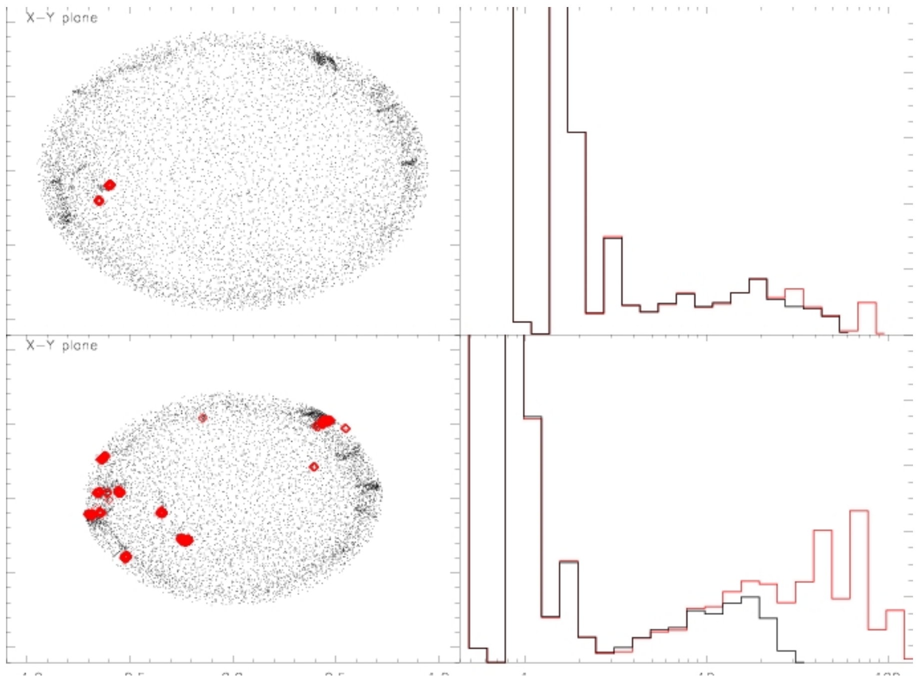

Figure 6: The upper left resp. lower left subplots show the distribution of 8.765 resp. 7.620 particles projected on the X-Y plane in a shell of size 10 h^{-1}kpc at $0.67R_{vir}$ resp. $0.89R_{vir}$. The particles with a nonzero star formation rate (SFR) are shown as diamonds. The local density of each particle is calculated by drawing a sphere of 3 h^{-1}kpc around it and deriving the spheres density. The upper right resp. lower right subplots show the resulting histograms for both shells. All density values are divided by the average density for each of the two shells. Next, particles with either a SFR or close (within 3 h^{-1}kpc) to one are removed from the data. For the remaining particles a histogram is also given in the right subplot. In the upper right histogram a small discrepancy between the two histograms becomes visible for overdensities $\Delta > 30$. In the lower right histogram the discrepancy grows clearly at $\Delta > 20$.

3.3 Probability

In terms of probability, one can consider the chance that an infalling dwarf galaxy encounters a region with a density of Δ times the average shell density. By using the properties of the infalling galaxy, we calculate the probability, P_{sp}, that cold gas will be stripped from the dwarf galaxy up to a radius R, given the background conditions of the progenitor halo. We couple the measurements of overdensities Δ with the homogeneous background model described in section 2.1. The properties of the infalling galaxies are described in the models of chapter 2.

The stripping probability, P_{sp}, might eventually depend on the removal radius R_{rem}. In the outer parts of the halo Fig. 6 shows that there are less satellite galaxies and the removal radius has a small influence. But when shells closer to the halo centre are examined, the number of halo galaxies increases and the removal radius becomes more important. Therefore, we take this into account by varying R_{ram} in the range $1-5$ h^{-1}kpc.

Two background density models are considered:

1. The gas in the halo is distributed homogeneously and is analytically described using a NFW profile. The procedure is described in chapter 2.

2. The gas in the halo has an inhomogeneous distribution. The analytic NFW profile will be used to describe the *average* density at r_{per}. And the distribution of Δ overdensities obtained from the SPH simulation at $0.67R_{vir}$ and $0.89R_{vir}$ will be coupled to that.

P_{sp} is straight forward to compute for the first case, where the background density to strip gas from a dwarf galaxy is homogeneously distributed. Therefore, $P_{sp} = 1$ for all $r_{per} < r_{crit}$ and $P_{sp} = 0$ for all $r_{per} > r_{crit}$, where ram pressure forces and gravitational resistance are equal (see Eq. 12). This is also illustrated in Fig. 3.

In the second case, we know from the analytic models (Fig. 2), the value of the required ram pressure to strip gas up to a radius R from a dwarf galaxy. At fixed velocity the value of the required density is known and is used to calculate Δ_{req} which is analogous to eq. (13) defined as: $\Delta_{req} = \frac{\rho_{req}}{<\rho>}$. The average background density, $<\rho>$, comes from the NFW profile and depends on r_{per}. Using a MW sized halo with an inhomogeneous gaseous halo, Δ_{req} yields the required value of overdensity to strip gas from the dwarf at r_{per}. Finally, the probabilities to encounter regions with this overdensity is given by the Δ distributions computed for each shell. The values for the overdensity Δ are given and P_{sp} can be calculated by $P(\Delta \geq \Delta_{req})$.

At a given radius R within the dwarf, the stripping probability will depend on the pericenter distance and on the dwarf velocity. Some variations on $P(\Delta \geq \Delta_{req})$ are expected for different assumption of the removal radius R_{rem}. We have computed the probabilities for a dwarf model to lose partly its gas with $R > R_{sp}$ due to stripping for several combinations of pericenter radius, velocities, R_{rem}. Our results are summarized in Table 4.

scaled pericenter radius (in units of R_{vir})	stripping radius (h^{-1}kpc)	velocity (km s^{-1})	$P(\Delta \geq \Delta_{req})$
0.61 - 0.73	R_d	100	$0.0823 - 0.217$
		150	$0.192 - 0.328$
		200	$0.218 - 0.360$
	R_h	100	$0.220 - 0.358$
		150	$0.271 - 0.413$
		200	$0.654 - 0.729$
0.80 - 0.98	R_d	100	$0.0398 - 0.0463$
		150	$0.107 - 0.113$
		200	$0.138 - 0.145$
	R_h	100	$0.127 - 0.134$
		150	$0.187 - 0.195$
		200	$0.359 - 0.365$

Table 4: $P(\Delta \geq \Delta_{req})$ values as function of the normalized pericenter radius, stripping radius of the dwarf R_{sp}, background velocity v and the removal radius R_{rem}. For R_{sp} two values are chosen: the scale length of the disk ($R_d = 1.0$ h^{-1}kpc) and the half mass radius ($R_h = 1.7$ h^{-1}kpc). 3 Typical dwarf galaxy velocities are chosen. R_{rem} values of 1.0 and 5.0 h^{-1}kpc are chosen where 1.0 h^{-1}kpc resp. 5.0 h^{-1}kpc corresponds to the upper resp. under limit on the probability values.

The values from table 4 are plotted in Fig. 7 as a function of the normalized pericenter radius. The other background density model assuming a homogeneous background distribution is also shown in Fig. 7 as a box function.

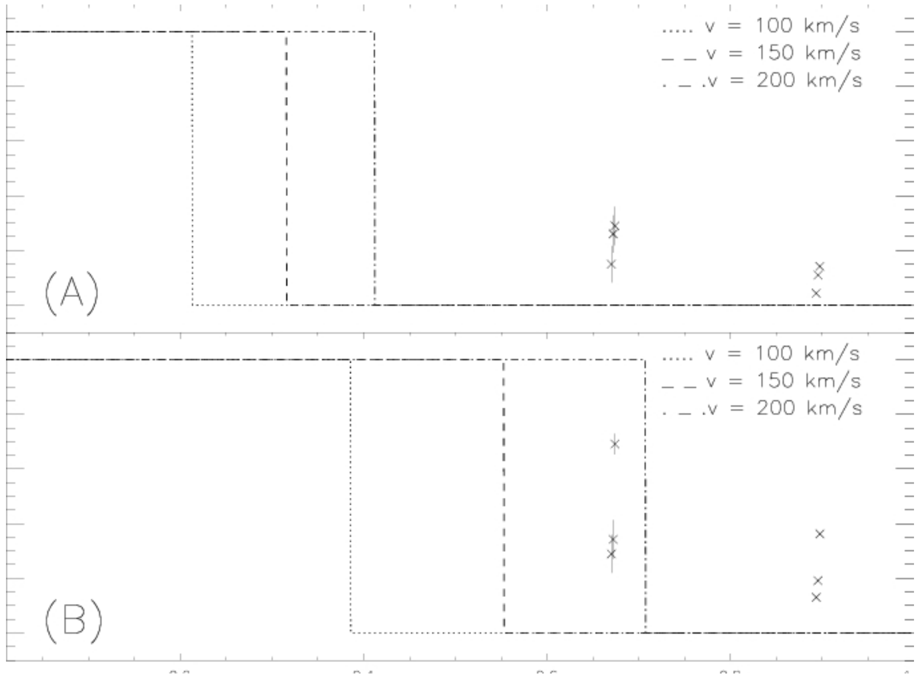

Figure 7: Probabilities of cold gas being stripped away from the infalling dwarf beyond a cylindrical radius $R = 1.0$ (A) and 1.7 (B) h^{-1}kpc , as a function of pericenter radius normalized by the virial radius. The box function shows the probabilities for the homogeneous background model for three different velocity values which increase from left to right. The dots with an error bar indicate the probabilities calculated for the inhomogeneous background model at 0.67 R_{vir} and 0.89 R_{vir} for three velocities (Table 4), where the error bar results from the range of values for R_{rem}.

Table 4 and Fig. 7 show that cold gas can be stripped up to the disk scale length even for dwarfs on external orbits. For example for orbits with pericenter of $\sim 0.67R_{vir}$ and a typical velocity of 200 km s^{-1}, the probability lies between 22% and 36%. For orbits with a larger pericenter ($\sim 0.89R_{vir}$), the probability has still a non-negligible value of $\sim$ 14% in our model.

4 Discussion and conclusion

In this report we have addressed the problem of the origin of the present day gas-poor dSph satellites in the outer regions of our MW halo, where ram pressure stripping, rather than tidal stripping, is assumed to be the main process in cold gas removal. We have examined the interaction between an infalling gas-rich dIrr satellite and the media of a MW like (gaseous) halo. Our contribution is original in the sense that we have analysed the effect of local inhomogeneities of the gaseous host halo on the amount of cold gas being removed from the satellite. We found that inhomogeneities in the outer regions of the host halo provides a plausible scenario in explaining the cold gas removal from dIrr satellites with large pericenter passages.

The parameters for the model of the satellite galaxy listed in Table 1 are taken from a GA2 + semi-analytic simulation of a ΛCDM universe. Those parameters are comparable to the GR8 model (Mayer [21]) and correspond to faint dIrr galaxies with very high central DM densities providing most of the gravitational resistance. Furthermore, our model for the host galaxy representing the MW follows a NFW profile and its normalization is in agreement with observations where the values for the background density are poorly constraint by other authors (Mastropietro et al. [20]; Sembach et al. [28]; Putman et al. [27]) in the range of $10^{-4} - 10^{-5}$ cm^{-3} for distances in the range of $50 - 100\ h^{-1}$kpc. Besides the substructure in density, we have also explored the variations in the relative velocity between the infalling satellite galaxy and the background medium, defined as: $\delta v = |v_{sat} - v_{bg}|$. Tonnesen & Bryan [30] examined the impact of the intracluster medium (ICM) on ram pressure stripping. These authors showed that in the outer regions of a cluster the variation in ram pressure stripping is dominated by ICM density variations rather than variations in δv. They also found a weak correlation between the motion of the ICM gas and the galaxy velocity. We expect gas within the virial radius to be in approximate hydrostatic equilibrium and therefore with negligible velocity compared to the satellite orbiting velocity. The explored range of velocities $100 - 200$ km s^{-1} are in agreement with the expected orbits of dwarfs in a ΛCDM universe.

In the last part of chapter 2 we showed that ram pressure forces are not effective beyond $r > 0.4\ r_{vir}$ for our analytic model. But if an inhomogeneous distribution of gas is assumed, the results show a non-negligible probability of effective ram pressure stripping even near r_{vir}. We warn however that our results show dependencies on the criteria assumed to remove satellite galaxies from the host. We have quantified such variations by varying the removal radius R_{rem} between $1 - 5h^{-1}$kpc. It is possible that this mechanism also acted on some of the MW dSphs located in the outskirts ($1 - 4R_{vir}$) like Leo I, Cetus and Tucana. They may have been transformed in morphology by orbiting through local dense environments instead of having several close pericenter passages in the past. In fact, there have been claims of such mechanism at work in the further away dIrr Pegasus dwarf (McConnachie et al. [24]). Future studies on their orbits and the use of very high resolution simulations including the inhomogeneity of the background media may shed light on the origin of today's dSphs.

References

[1] Abadi M.G., Moore B., Bower R.G., 1999, MNRAS 308, 947

[2] Binney J., Tremaine S., 2008, Galactic Dynamics (second edition), Princeton University Press, Princeton NJ

[3] Bryan G., Norman M., 1998, ApJ 495, 80

[4] Bullock J.S., 2001, MNRAS 321, 559B

[5] Cavaliere A., Fusco-Femiano R., 1976, A&A 49, 137

[6] Dressler A., 1980, ApJ 236, 351

[7] Eke V.R., Navarro J.F., Frenk C.S., 1998, ApJ 503, 569

[8] Fang T., Mckee C.F., Canizares C.R., Wolfire M., 2006, ApJ 644, 174

[9] Grcevich J., Putman M.E., 2009, ApJ 696, 385G

[10] Grebel E.K., Gallagher J.S., Harbeck D., 2003, AJ 125, 1926

[11] Gunn & Gott 1972, ApJ 176, 1

[12] Hernandez X., Gilmore G., Valls-Gabaud D., 2000, MNRAS 317, 831

[13] Hernquist L., 1993, ApJS 86, 389

[14] Kaufmann T., Bullock J.S., Maller A.H., Fang T., Wadsley J, 2008, MNRAS, accepted

[15] Larson R.B., Tinsley B.M., Caldwell C.N., 1980, ApJ 237, 692

[16] Li Y., Helmi A., 2008, MNRAS 385, 1365L

[17] Lin D.N.C., Faber S.M., 1983, ApJ 266, 21L

[18] Lokas E.L., Mamon G.A., 2001, MNRAS 321, 155L

[19] Maller A.H., Bullock J.S., 2004, MNRAS 355, 694

[20] Mastropietro C., Moore B., Mayer L., Wadsley J., Stadel J., 2005, MNRAS 363, 509M

[21] Mayer L., Governato F., Colpi M., Moore B., Quinn T., Wadsley J., Stadel J., Lake G., 2001, ApJ 559, 754

[22] Mayer L., Near-Field Cosmology with Dwarf Elliptical Galaxies, Proceedings IAU Colloquium No. 198, 2005,

[23] Mayer L., Mastropietro C., Wadsley J., Stadel J., Moore B., 2006, MNRAS 369, 1021

[24] McConnachie A.W., Venn K.A., Irwin M.J., Young L.M., Geehan J.J., 2007, ApJ 671, 33L

[25] Murali C., 2000, ApJ 529, L81

[26] Navarro, J.F., Frenk C.S., White, S.D.M., 1996, ApJ 462, 563

[27] Putman M.E., Bland-Hawthorn J., Veilleux S., Gibson B.K., Freeman K.C., Maloney P.R., 2003, ApJ 597, 948

[28] Sembach K.R., Wakker B.P., Savage B.D., Richter P., Meade M., Shull J.M., Jenkins E.B., Sonneborn G., Moos H.W, 2003, ApJS 146, 165S

[29] Stoehr F., White S.D.M., Tormen G., Springel V., 2002, MNRAS 335, 84L

[30] Tonnesen S., Bryan G.L., 2008, ApJ 684L, 9T